Spectral Asymptotics of the Laplacian on Surfaces of Constant Curvature

Timothy S Murray & Robert S Strichartz

May 2015

Abstract

The purpose of this paper is to explore the asymptotics of the eigenvalue spectrum of the Laplacian on 2 dimensional spaces of constant curvature. We computed and analyzed the eigenvalue spectra of several different regions in Euclidean, Hyperbolic, and Spherical space under Dirichlet, Neumann, and mixed boundary conditions in order to observe the how closely the spectra conform to Weyl's Asymptotic Law and subsequent advances, while simultaneously using the Law to determine the accuracy of our new methods of computing Hyperbolic and Spherical spectra.

1 Introduction

The purpose of this paper is to present numerical evidence for a conjecture on the spectral asymptotics of the Laplacian on a surface of constant curvature presented by the second author in [S]. The conjecture was initially limited to surfaces of either zero or constant positive curvature, but we present strong evidence that it should also be valid in the case of constant negative curvature. Results of Bleher [B] show that it cannot be valid for surfaces of variable curvature, and indeed we give some numerical examples in the variable curvature case that highlight the difference.

We consider surfaces S of finite area A with boundary ∂S of finite perimeter P that is made up of a finite number of smooth curves meeting at angles $\{\theta_j\}$. Simple examples are triangles and discs in either the Euclidean plane, the sphere, or hyperbolic 2-space. We will also look at more complicated examples where S is not simply connected and has non-convex boundary. We consider the standard Laplacian Δ with either Dirichlet (D), Neumann (N), or mixed boundary conditions (D on a portion of the boundary with perimeter P_D, and N on the remaining portion of the boundary with perimeter P_N). We let $\{\lambda_j\}$ be the set of eigenvalues $-\Delta u_j = \lambda_j u_j$ repeated according to multiplicity, so the λ_j are all nonnegative and $\lambda_j \to \infty$ as $j \to \infty$. The eigenvalue counting function is defined as

(1.1) $N(t) = \#\{\lambda_j \leq t\}$
(Note that some references will use $\lambda_j \leq t^2$ instead). The well-known Weyl asymptotic formula $N(t) \sim \frac{A}{4\pi}t$ was refined by Ivvii [I] to

(1.2) $N(t) = \frac{A}{4\pi}t + \frac{P_N - P_D}{4\pi}t^{1/2}$
In [S] we proposed a still more refined asymptotic

(1.3) $\widetilde{N}(t) = \frac{A}{4\pi}t + \frac{P_N - P_D}{4\pi}t^{1/2} + C$
where the constant C will be explained in Definition 1.1 below. However, it is impossible to see the constant from $N(t)$ alone, since it is expected that

(1.4) $D(t) = N(t) - \widetilde{N}(t)$ will have at least growth $O(t^{1/4})$. Instead we consider the ordinary average error

(1.5) $A(t) = \frac{1}{t}\int_0^t D(s)\,ds$.
We conjecture that this decays on the order of $O(t^{1/4})$, see Conjecture 1.2 below for a more detailed description. For this to be valid we need the correct value for the constant. We note that a different kind of average, the trace of the heat kernel

(1.6) $h(t) = -\sum_j e^{-t\lambda_j}$
(as $t \to 0$) has been estensively studied, beginning with the famous paper of Mark Kac [K] and continuing with [BS],[Bn] and [G]. We note that the trace of the heat kernel is a much smoother average, and so it erases the oscillatory behavior that we will see in $A(t)$.

The method we use to numerically approximate the spectrum of the Laplacian is extremely straightforward. We use the finite element solver built into MATLAB. For surfaces in the plane we just have to give a description of the boundary. For surfaces in the hyperbolic plane or sphere we us a conformally flat coordinate system so the surface Laplacian becomes a scalar multiple of the Euclidean Laplacian. By using the refinement option we obtain better and better approximations of smaller initial segments of the spectrum. Given the computation time constraints, this allows us to get confident approximations for only a couple hundred eigenvalues. We then use an ad hoc extrapolation method on the sequence of approximations with increasing refinements to get a slightly improved final approximation. We were pleasantly surprised to see that this small peek at an initial segment of the spectrum already yields strong evidence for the conjecture. In other words, it appears that the asymptotic regimine kicks in very early in the game. In the case of the Euclidean disc we have a better alternative method, since there the eigenvalues are given explicitly as squares of zeroes of Bessel functions of the first kind (D) or zeroes of derivatives of Bessel functions of the first kind (N). This allows us to go higher up in the spectrum with greater accuracy, and serves as a check on the size of the error obtained by the cruder method. Another check on error size is provided by doing the computations for the few triangles where the exact spectrum is known.

We now present the details concerning the constant C in (1.3)

Definition 1.1 : Let $K_2(S)$ denote the curvature of S, which is assumed to be constant, and let K_1 denote the curvature function on the smooth pieces of ∂S as viewed from S. Define

(1.7) $\varphi(\theta) = \frac{1}{24}(\frac{\pi}{\theta} - \frac{\theta}{\pi})$
Then

(1.8) $C = C_1 + C_2 + C_3$
where

(1.9) $C_3 = \frac{1}{12\pi} A K_2(S)$,

(1.10) $C_2 = \frac{1}{12\pi} \int_{\partial S} K_1$, and

(1.11) $C_1 = \sum_j \varphi(\theta_j)$ in the case of D or N boundary conditions throughout, or

(1.12) $C_1 = \sum \varphi(\theta'_j) + \sum(\varphi(2\theta''_j) - \varphi(\theta''_j))$ for mixed boundary conditions, where the corner angles are sorted into $\{\theta'_j\}$ where the same type of boundary condition is imposed on both sides of the corner, and $\{\theta''_j\}$ where opposite type boundary conditions are imposed on the two side arcs.

We note that in [S] we also allowed a finite number of cone point singularities on S with cone angles $\{\alpha_j\}$, and these contributed an additional term

(1.13) $\sum 2\varphi(\alpha_j/2)$
to C_1. However, we are unable to do our computations if there are cone point sungularities, so we can't test the conjecture in such cases.

Conjecture 1.2: a) Assume the curvature of S is zero or negative. Then there exists a uniformly almost periodic function g of mean value zero such that

(1.14) $A(t) = g(t^{1/2})t^{-1/4} + O(t^{-1/2})$ as $t \to \infty$.
b) Assume the curvature of S is positive. Then there exists a uniformly almost periodic funtion g of mean value zero such that

(1.15) $A(t) = g(t^{1/2}) + O(t^{-1/2})$ as $t \to 0$

We note that in [S] we conjectured that (1.14) and (1.15) are the first terms in an asymptotic expansion, but we are unable to test this here. Indeed, we cannot test the rate of decay in (1.14) and (1.15), since we don't know what g should be. So basically we will observe that $t^{1/4}A(t)$ in case a) and $A(t)$ in case b) appear to be bounded functions of t^2 with mean value zero that could reasonably be almost periodic. Since almost periodicity is a global property, there is no way to test it by examining a small portion of the graph. We will observe, however, that there is no discernable difference between examples where the almost periodicity is known to be true, and all the other examples.

2 Some Test Examples

In this section we discuss our results for a few examples of surfaces where the spectrum is known exactly.

Example 2.1: The Euclidean right isosceles triangle with Dirichlet boundary conditions

The set of eigenvalues is $\pi^2(j^2+k^2)$ for all pairs (j,k) of distinct positive integers. We will normalize all eigenvalues by dividing by π^2 so that we are dealing with integer values. In Table 2.1 we show the data for the first 10 eigenvalues (the full table is on the website at http://www.math.cornell.edu/ tmurray3014/DirEuc45Tri.html). In the first column we show the initial MATLAB computation of $\frac{\lambda_j}{\pi^2}$. In the next 6 columns we show the same value of after successive refinements. So the initial value of $\frac{\lambda_{10}}{\pi^2}$ is 44.931704, which is quite far from the true value of 37, but by the 6^{th} refinement the approximation has improved to 37.001949. The next column is our predicted value obtained by fitting the data x_n for refinements $n = 4, 5, 6$ to $x_n = x + cr^n$ and taking x for the prediction. In this case the prediction is 37.000001. If we look further up in the spectrum we can see eigenvalues with multiplicity 2. For example $\frac{\lambda_{133}}{\pi^2} = \frac{\lambda_{134}}{\pi^2} = 377$. At refinement 4 the two values are 380.03292 and 380.1314. Not very close to each other and far off from the true value. At refinement 5 the two values are 377.7568 and 377.7816, closer to the true value but still not too close to each other. The predicted values are 376.9999 and 376.9998. Even though the order gets switched, the error is still quite acceptable.

	Initial	Refinement 1	2	3	4	5	Predicted
1	5.135899	5.034796	5.008795	5.002208	5.000138	5.000138	5
2	10.57357	10.14484	10.03646	10.00914	10.00057	10.00057	10
3	13.90424	13.22818	13.05738	13.01438	13.0009	13.0009	13
4	18.67836	17.41949	17.10514	17.02632	17.00165	17.00165	17
5	22.34258	20.58065	20.14513	20.03631	20.00227	20.00227	20
6	28.51405	25.87608	25.21908	25.05481	25.00343	25.00343	25
7	29.79926	26.94736	26.23707	26.05934	26.00371	26.00371	26
8	33.5825	30.15266	29.28919	29.07244	29.00453	29.00453	29
9	40.60456	35.64851	34.41145	34.10291	34.00644	34.00644	34
10	44.9317	38.99349	37.4981	37.12463	37.00779	37.00779	37
...	...	...	...	...	...	...	...
133	0	0	0	389.6568	377.7568	377.7568	376.9999
134	0	0	0	398.8737	377.7816	377.7816	376.9998

Table 2.1

In Figure 2.1 we show the graphs of

1) $N(t)$

2) $D(t) = N(t) - \widetilde{N}(t)$

3) $A(t) = \frac{1}{t}\int_0^t D(s)ds$

4) $t^{\frac{1}{4}}A(t)$

5) $t^{\frac{1}{4}}A(t^2)$

6) $\frac{1}{t-a}\int_a^t s^{\frac{1}{2}}A(s^2)ds$ for $a =$ needs to be filled in

We used the exact values for the first approximately 150 eigenvalues. A quick look at these graphs yields some simple observations. The graph 1) shows that $N(t)$ grows approximately linearly, while 2) shows that $D(t)$ grows at a relatively slow rate. the graph 3) suggests that $A(t)$ is converging to 0 at a slow rate, while graph 4) confirms that $O(t^{-\frac{1}{4}})$ is a plausible decay rate. The function in graph 5) is known to be converging to an almost periodic function g(t), but this is not apparent from the graph. Presumably the almost periods are too large to show up in the range of data we have plotted. On the other hand, graph 6) gives strong evidence that the almost periodic function has mean value 0.

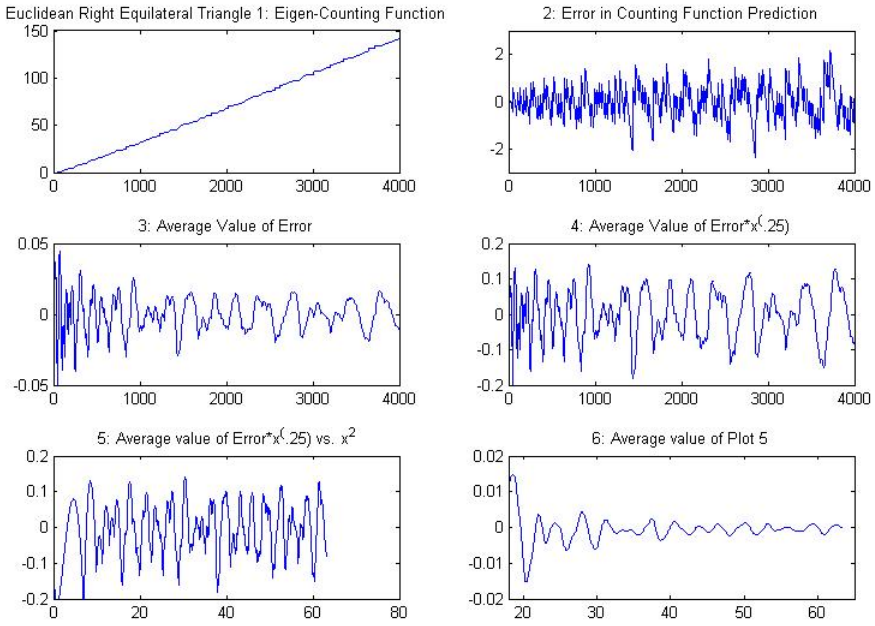

Figure 2.1

In Figure 2.2 we display the set of differences $\frac{(\lambda_{k+1}-\lambda k)}{\pi^2}$, both as a cumulative sum and a histogram. Since these differences are all integers there is no question

about the choice of bin sizes for the histogram. It is not clear from the limited data how the histogram will behave in the limit. The fact that the bin values are very far from being decreasing is very intriguing. Ultimately it should be an interesting problem in number theory to find any pattern.

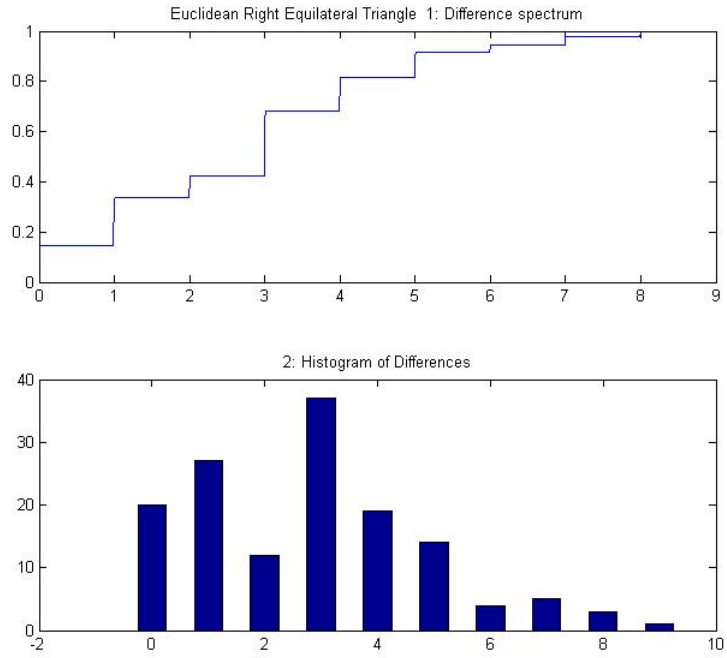

Figure 2.2

Example 2.2: The Euclidean equilateral triangle with Dirichlet boundary conditions.

Here the eigenvalues are known to be the values $(\frac{4}{3}\pi)^2(j^2+k^2+jk)$ for the positive integers j,k. This typically produces multiplicity 1 when $j=k$ and multiplicity 2 when $j \neq k$. Here we only used 5 refinements. Table 2.2 and Figures 2.3 and 2.4 show the same information for this example as before. For $\lambda_{119} = \lambda_{120} = 219$ our predicted values are 219.0009455 and 219.0005973 while on the 5^{th} refinement they are 219.4644686 and 219.4662058. The qualitative features of Figures 2.3 and 2.4 are much the same as Figures 2.1 and 2.2.

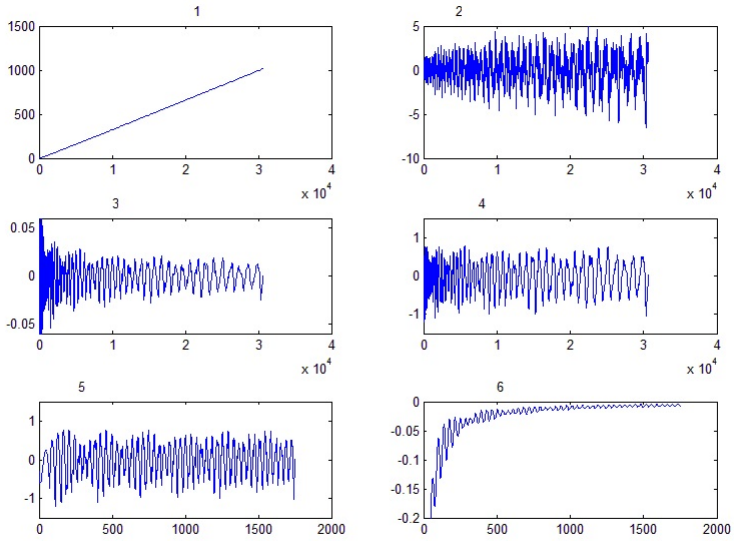

Figure 2.3

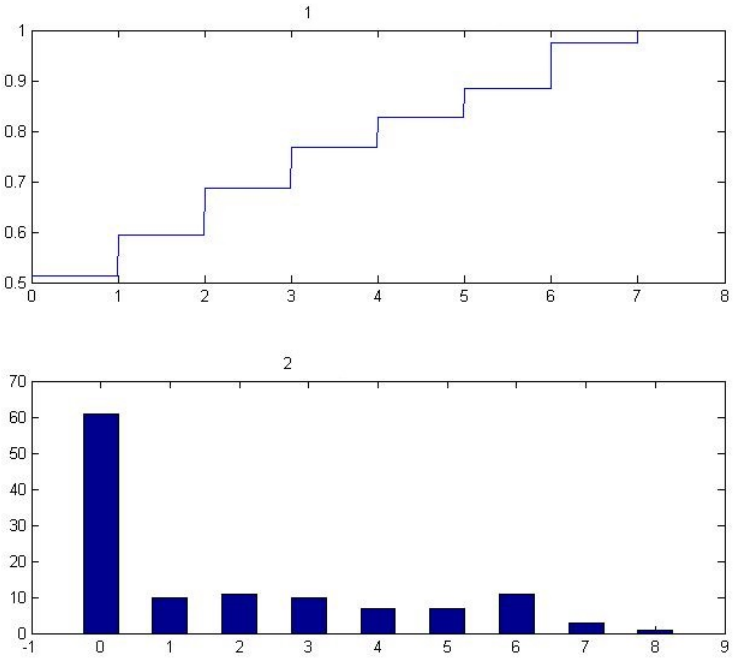

Figure 2.4

	Initial	Refinement 1	2	3	4	5	Predicted
1	3.087325	3.022238	3.005611	3.001408	3.000088	3.000088	3.000001
2	7.441032	7.111702	7.028133	7.007054	7.000441	7.000441	7.000003
3	7.498712	7.124316	7.03113	7.007791	7.000487	7.000487	7.000003
4	13.46061	12.36126	12.09015	12.02254	12.00141	12.00141	12.00001
5	14.64219	13.40837	13.10213	13.02555	13.0016	13.0016	13.00001
6	14.7099	13.42404	13.10604	13.02654	13.00166	13.00166	13.00001
7	22.38661	19.84793	19.2122	19.05312	19.00332	19.00332	19.00002
8	22.75809	19.94249	19.23499	19.05874	19.00367	19.00367	19.00002
9	25.32908	22.05932	21.26293	21.06566	21.0041	21.0041	21.00002
10	25.35513	22.07051	21.26635	21.06656	21.00416	21.00416	21.00002

Table 2.2

Example 2.3: The Euclidean disc with Dirichlet boundary conditions.

We take the radius to be one since all discs have eigenvalues that scale by the radius. In this case the eigenvalues are the squares of the zeroes of the Bessel functions J_k for nonnegative integers k with multiplicity one for $k = 0$ and multiplicity two for $k \geq 1$. It is possible to get accurate values of these zeros so we have exact values for the first 660 eigenvalues. In this example $\widetilde{N}(t) = \frac{1}{4}t - \frac{1}{2}\sqrt{t} + \frac{1}{6}$. Note, however, that the validity of the conjecture is not known in this example. In Table 2.3 we show the first 10 computed approximations with 4 refinements. The table also lists the zeros of the Bessel function and the values k and n for $J_k(z_n) = 0$. The accuracy of our predictions are worse than in the triangle examples. For example $\lambda_{149} = \lambda_{150} = 646.7022512 = (z_6)^2$ for $J_5(z_6) = 0$ has fairly accurate predicted values 646.7227695 and 646.7146116, while $\lambda_{212} = \lambda_{213} = Countin910.7757336 = (z_5)^2$ for $J_{11}(z_5) = 0$ has unacceptable predicted values 910.4406915 and 906.2756139.

Figure 2.5 displays the same graphs as before using the exact values. We note that graph 5) is just as plausibly an asymptotic almost periodic function as the same graphs in the triangle cases where we know the function is asymptotically almost periodic. (NOTE: for this next part, I typed it up but you should look at the re-done counting graphs for the Dirichlet counditions Euclidean disc) On the other hand, graph 6) shows a much slower rate of decay than in the triangle cases. It is still plausible that this gives supportive evidence that the presumed almost periodic function has mean value zero, but the evidence is not decisive. Figure 2.6 show the eigenvalue difference. In this case the histogram seems to have a different appearance than for the triangle cases, but now the result is sensitive to the choice of bin size.

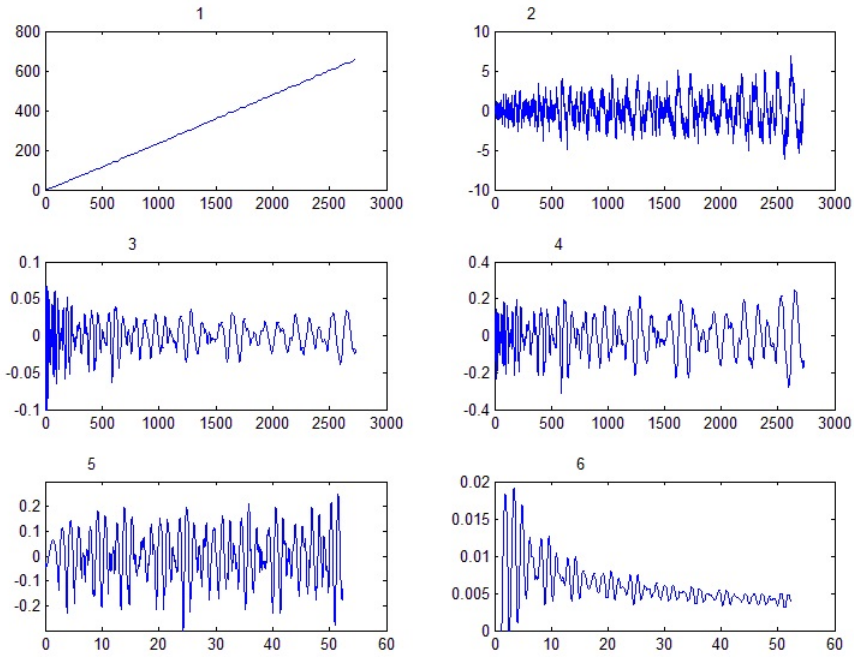

Figure 2.5

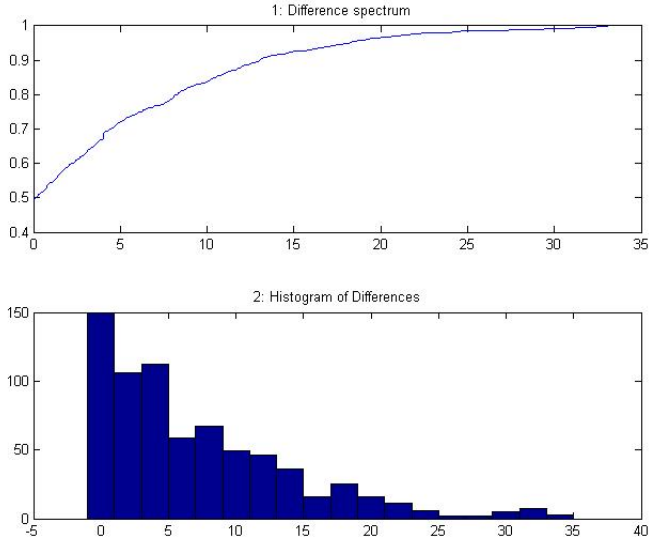

Figure 2.6

Example 2.4: Euclidean disc with Neumann boundary conditions (again with radius one).

In this case $\lambda = (z_n)^2$ where $J_k'(z_n) = 0$. Here we were able to obtain the exact values for the first 550 eigenvalues. Table 2.4 and Figures 2.7 and 2.8 show the corresponding data with $\widetilde{N}(t) = \frac{1}{4}t + \frac{1}{2}\sqrt{t} + \frac{1}{6}$. The qualitative features observed for the previous example are evident here as well.

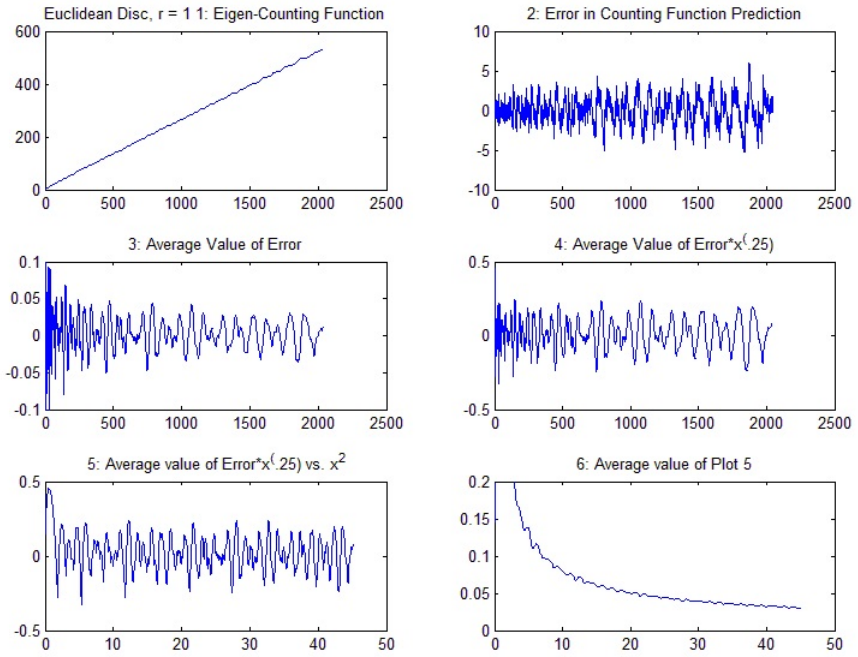

Figure 2.7

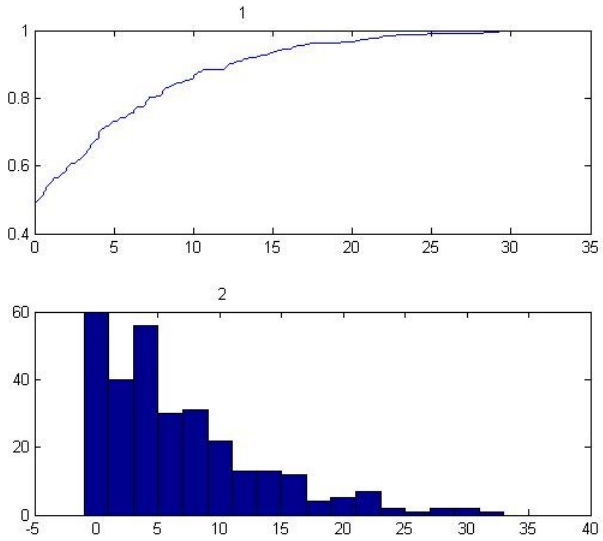

Figure 2.8

3 Flat Surfaces

In this section we discuss examples of polygonal surfaces in Euclidean space. In particular we examined examples of nonconvex surfaces, surfaces with angles exceeding π, and surfaces that are not simply connected. There are still more examples on the website [W]. For each example we give the beginning of the list of eigenvalues, and the analogs of Figures 2.1 and 2.2.

Example 3.1: Triangle with Dirichlet boundary conditions.

The angles are $\theta_1 = \frac{\pi}{4}, \theta_2 = \frac{\pi}{5}, \theta_3 = \frac{11\pi}{20}$ and

$$\widetilde{N}(t) = \frac{\sin\theta_2 \sin\theta_1}{8\pi \sin\theta_3} t - \frac{\frac{\sin\theta_1}{\sin\theta_3}\sqrt{t} + \frac{\sin\theta_2}{\sin\theta_3} + 1}{4\pi} + \frac{9}{22}$$

Here we used the first 130 calculated eigenvalues, as accuracy begins to break down after that point. The graphs in Figures 3.1 and 3.2 are analogous to those in Figures 2.1 and 2.2, respectively, and show similar behavior.

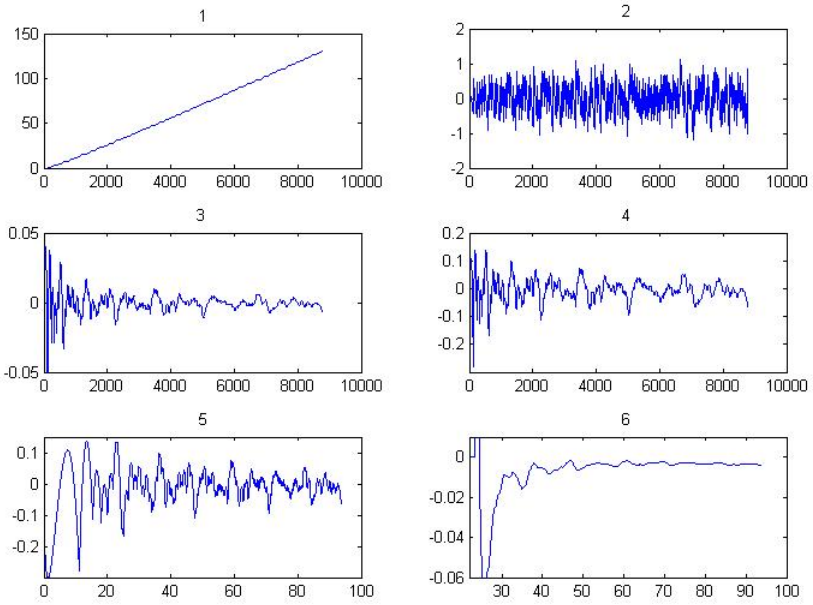

Figure 3.1

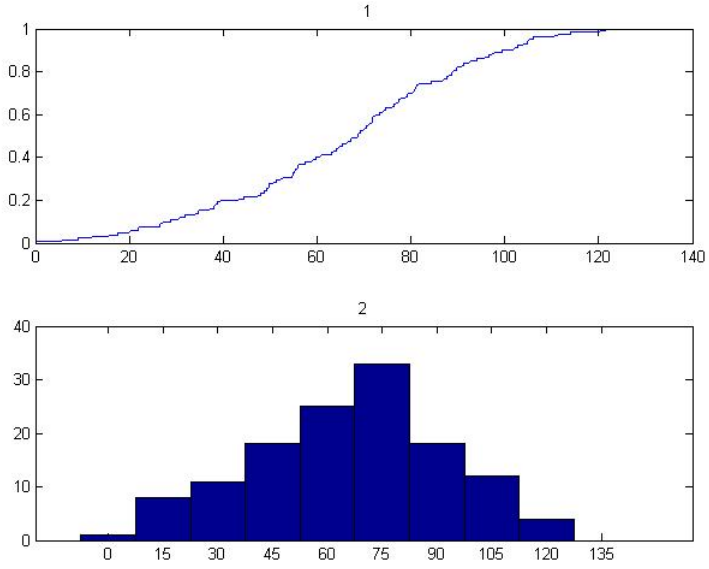

Figure 3.2

Example 3.2: Triangle with Neumann boundary conditions.

This is the same triangle as above, with

$$\widetilde{N}(t) = \frac{\sin\theta_2 \sin\theta_1}{8\pi \sin\theta_3} + \frac{\frac{\sin\theta_1}{\sin\theta_3}t + \frac{\sin\theta_2}{\sin\theta_3} + 1}{4\pi}\sqrt{t} + \frac{9}{22}$$

Here we used the first 150 calculated eigenvalues. The graphs in Figures 3.3 and 3.4 are analogous to Figures 3.1 and 3.2 and display the same behavior, except that in graph six of Figure 3.3 the graph is decreasing to 0, whereas it is increasing to zero in Figure 3.1. This difference is a result of the boundary conditions and is mirrored in all graphs of the same shape under Dirichlet and Neumann boundary conditions.

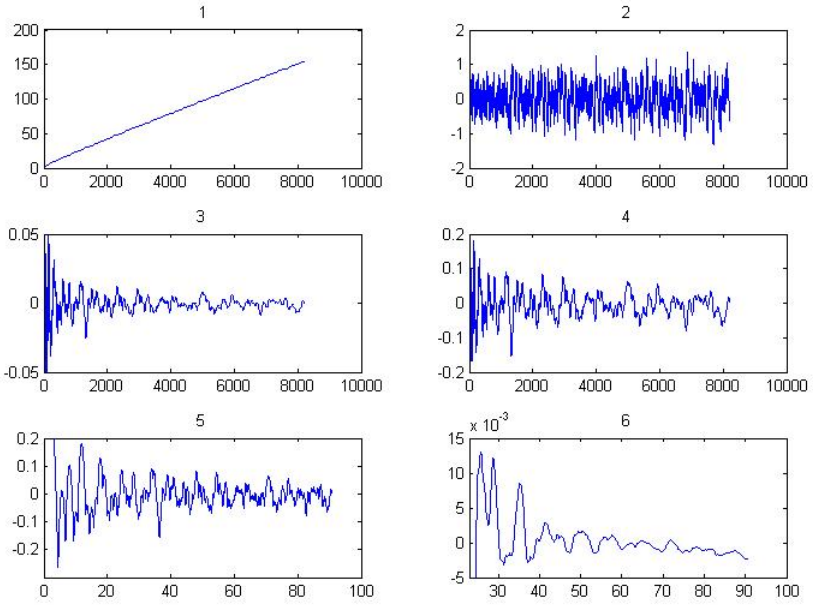

Figure 3.3

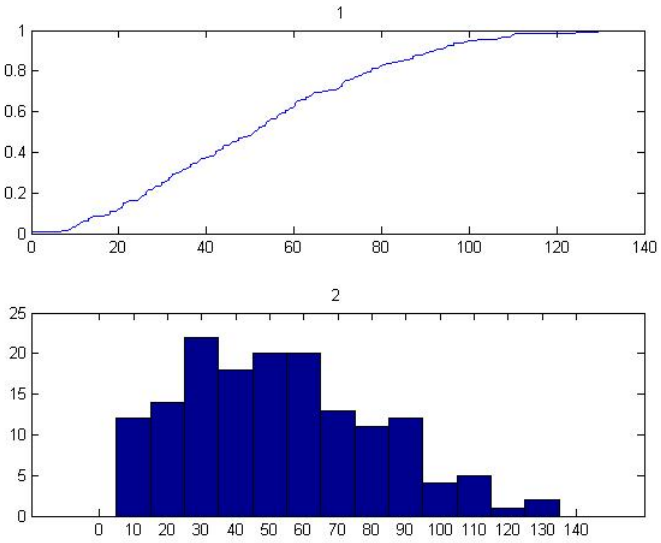

Figure 3.4

Example 3.3: Triangle with mixed boundary conditions.

With the same triangle, we impose Dirichlet boundary conditions on s_1 and s_2 and Neumann boundary conditions on s_3. Here

$$\widetilde{N}(t) = \frac{\sin\theta_2 \sin\theta_1}{8\pi \sin\theta_3} t - \frac{\frac{\sin\theta_1}{\sin\theta_3}\sqrt{t} - \frac{\sin\theta_2}{\sin\theta_3} + 1}{4\pi}\sqrt{(t)} + \frac{189}{110}$$

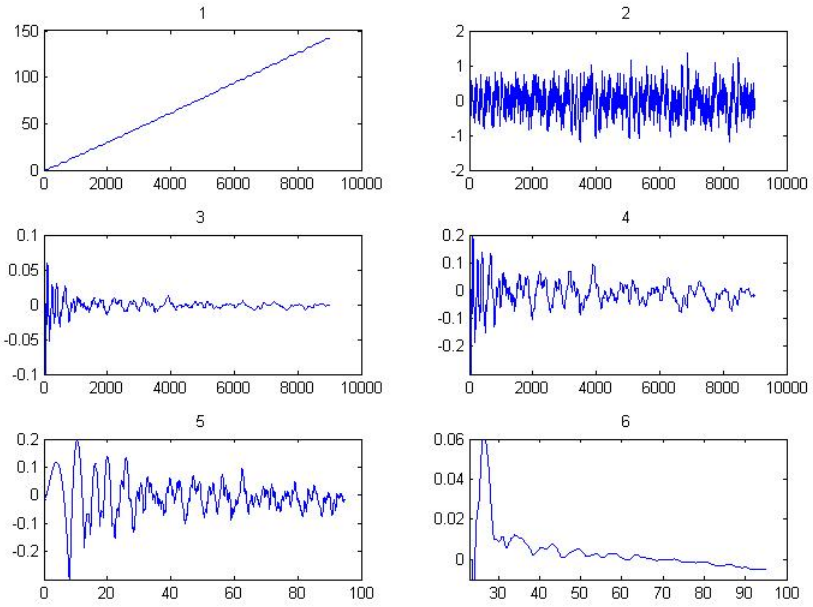

Figure 3.5

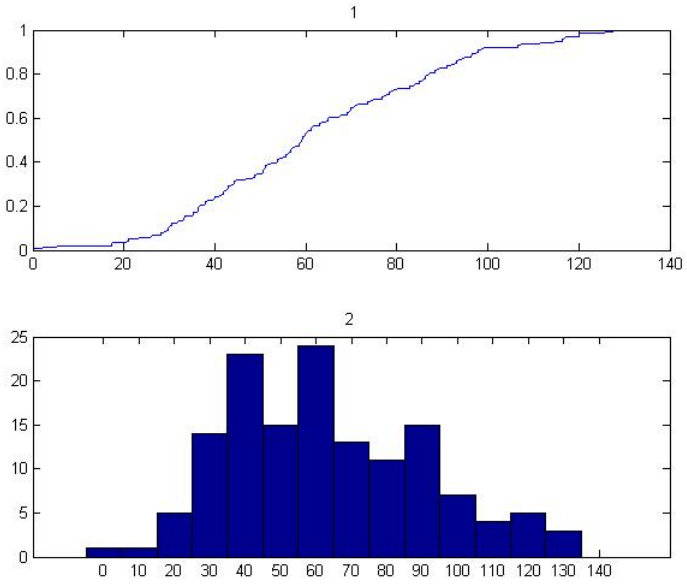

Figure 3.6

Example 3.4: Arrowhead with Dirichlet boundary conditions (see Figure 3.7)

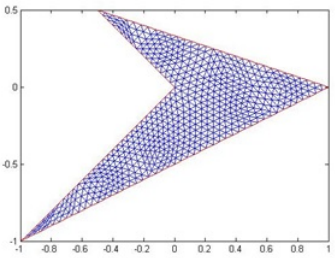

Figure 3.7

Here the sides are $s_1 = \frac{\sqrt{13}}{2}, s_2 = \frac{\sqrt{2}}{2}, s_3 = \sqrt{2}, s_4 = \sqrt{5}$. The angle θ_i joins sides s_i and s_{i-1}; θ_1 joins s_1 and s_4. The angle measures are $\theta_1 = \sin^{-1}\frac{1}{\sqrt{13}} + \sin^{-1}\frac{1}{\sqrt{5}}, \theta_2 = \cos^{-1}(\frac{s_1^2+s_2^2-1}{2s_1s_2}), \theta_4 = \cos^{-1}(\frac{s_3^2+s_3^2-1}{2s_3s_4}), \theta_3 = 2\pi - \theta_1 - \theta_2 - \theta_4$, and $\theta_3 > \pi$. We then have

$$\widetilde{N}(t) = \frac{\sqrt{\frac{s_1+s_2+1}{2}(s_1+\frac{s_2}{2}+1)(\frac{s_1}{2}+s_2+1)(s_1+s_2+\frac{1}{2})}+\sqrt{\frac{s_3+s_4+1}{2}(s_3+\frac{s_4}{2}+1)(\frac{s_3}{2}+s_4+1)(s_3+s_4+\frac{1}{2})}}{4\pi}t - \frac{\sum_{i=1}^4 s_i}{4\pi}\sqrt{t} + \frac{\sum_{i=1}^4 \theta_i}{24}$$

Figures 3.8 and 3.9 are analogous to the graphs we have seen before, and we can see that they display the same behavior.

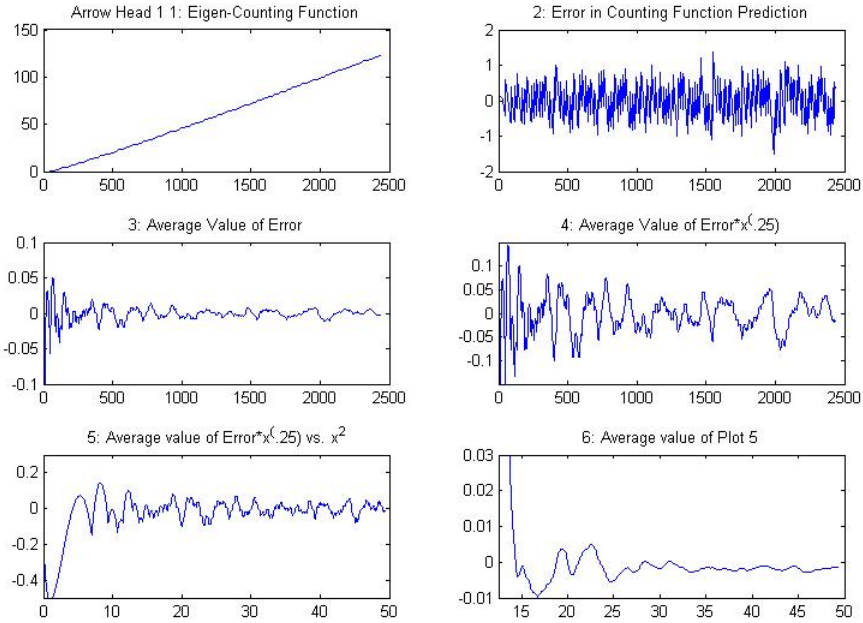

Figure 3.8

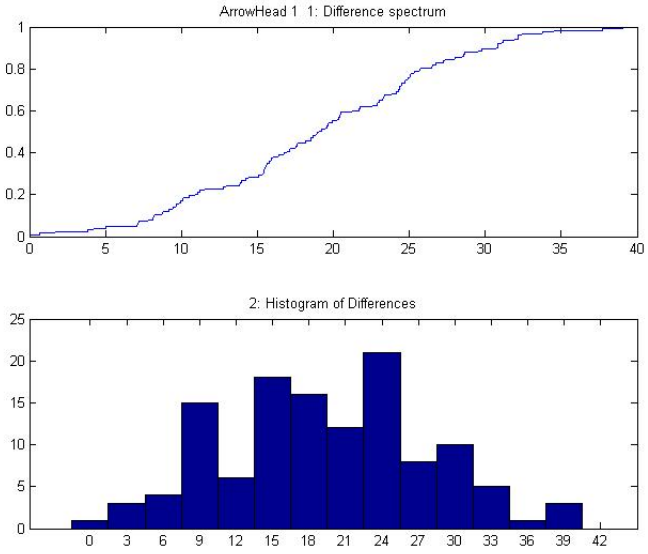

Figure 3.9

Example 3.5: Difference between triangles with Dirichlet boundary conditions (see Figure 3.10)

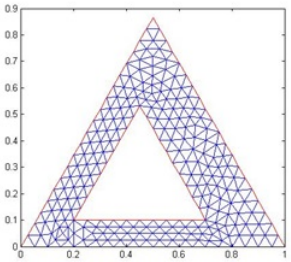

Figure 3.10

This is not simply connected. The angles of the interior triangle are viewed from the surface and hence are the exterior angles. We need to keep the vertices of the inner triangle a reasonable distance from the edges of the outer triangle in order to have reasonable accuracy in computing eigenvalues. Note that the formula $\widetilde{N}(t) = \frac{3\sqrt{3}}{64\pi}t - \frac{9}{8\pi}\sqrt{t} + \frac{1}{15}$ is independent of the location and orientation of the inner triangle.

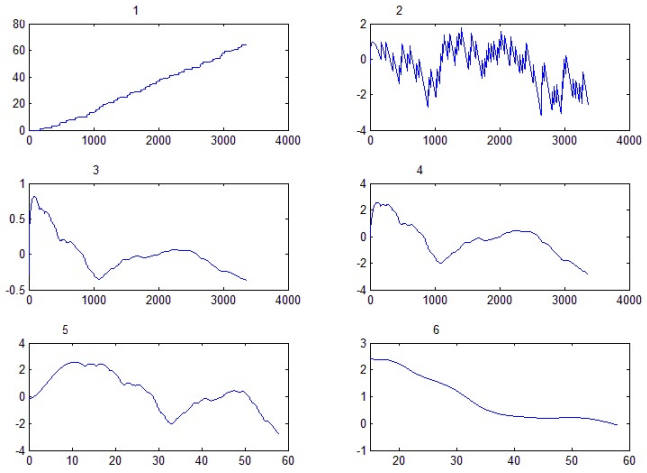

Figure 3.11

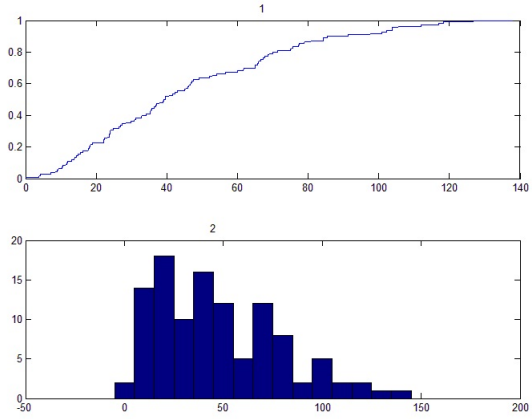

Figure 3.12

Example 3.6: Regular pentagon with Dirichlet boundary conditions.

Here $\widetilde{N}(t) = \frac{\sqrt{5(5+2\sqrt{5}}}{16\pi}t - \frac{5}{4\pi}\sqrt{t} + \frac{2}{9}$. Note that there are many eigenvalues of multiplicity two, due to the D_5 symmetry group. This gives us a reasonable tool for assessing the accuracy of our computations (since MATLAB does not select symmetric triangulations).

	Initial	Refinement 1	2	3	4	5	Predicted
1	11.14793	11.03526	11.00624	10.99889	10.99704	10.99658	10.99643
2	28.80056	28.04273	27.85074	27.80238	27.79025	27.78721	27.7862
3	28.81714	28.04763	27.85201	27.8027	27.79033	27.78723	27.7862
4	52.41101	50.06061	49.47096	49.323	49.28594	49.27667	49.27358
5	52.57104	50.10611	49.48295	49.32606	49.28671	49.27686	49.27359
6	61.58734	58.21567	57.37533	57.16477	57.11204	57.09885	57.09447
7	84.93856	78.95964	77.47257	77.1007	77.00764	76.98437	76.97664
8	85.06669	78.9798	77.47749	77.10193	77.00795	76.98445	76.97664
9	99.43871	91.724	89.80689	89.32718	89.2071	89.17706	89.16708
10	100.1192	91.89246	89.84908	89.33775	89.20975	89.17773	89.16708

Table 3.2

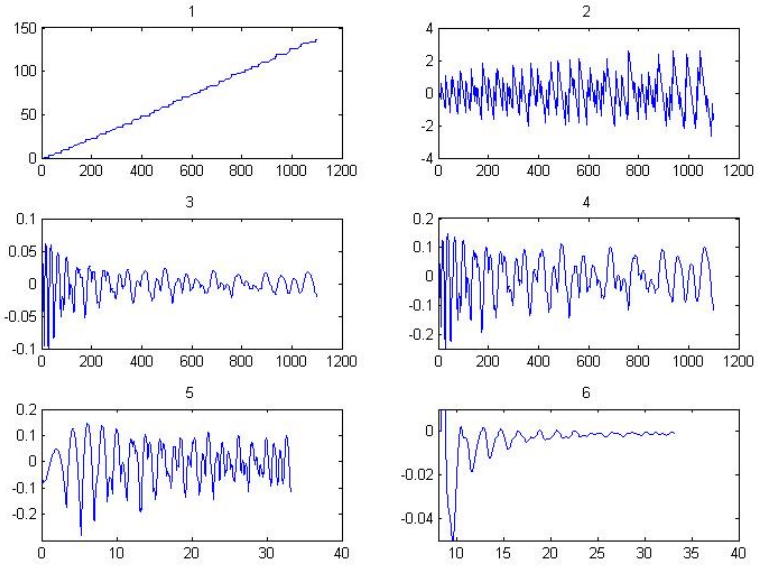

Figure 3.13

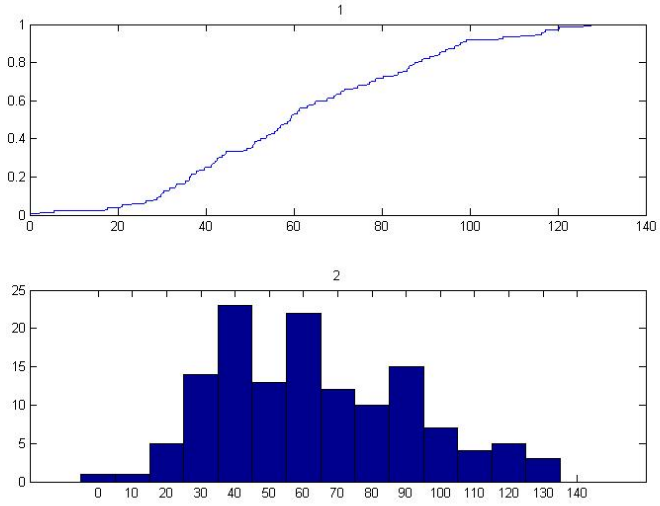

Figure 3.14

Example 3.7: Regular hexagon with Dirichlet boundary conditions.

Here $\widetilde{N}(t) = \frac{3\sqrt{3}}{8\pi}t - \frac{3}{\pi}\sqrt{t} + \frac{5}{24}$. Note that all Dirichlet eigenfunctions of the equilateral triangle extend by odd reflections to Dirichlet eigenfunctions of

the hexagon with the same eigenvalue. In our table of eigenvalues we therefore divide by $(\frac{4}{3}\pi)^2$ so that these eigenvalues become integers. This gives us an accuracy check. We have a D_6 symmetry group so that most eigenvalues have multiplicity two.

	Initial	Refinement 1	2	3	4	5	Predicted
1	0.4136213	0.4093449	0.4082004	0.4079053	0.4078305	0.4078117	0.4078055
2	1.069612	1.042747	1.035759	1.03398	1.033532	1.033419	1.033382
3	1.07095	1.043083	1.035843	1.034001	1.033537	1.033421	1.033382
4	1.968578	1.880006	1.857227	1.851466	1.850018	1.849655	1.849534
5	1.969445	1.880229	1.857298	1.851485	1.850023	1.849656	1.849534
6	2.288059	2.175413	2.146518	2.139204	2.137365	2.136905	2.136751
7	2.976487	2.782209	2.731673	2.718854	2.715627	2.714818	2.714549
8	3.328669	3.08177	3.020466	3.005122	3.001281	3.00032	3
9	3.808021	3.523318	3.450285	3.431787	3.427136	3.42597	3.425581
10	3.816109	3.524926	3.450607	3.43186	3.427153	3.425974	3.425581

Table 3.2

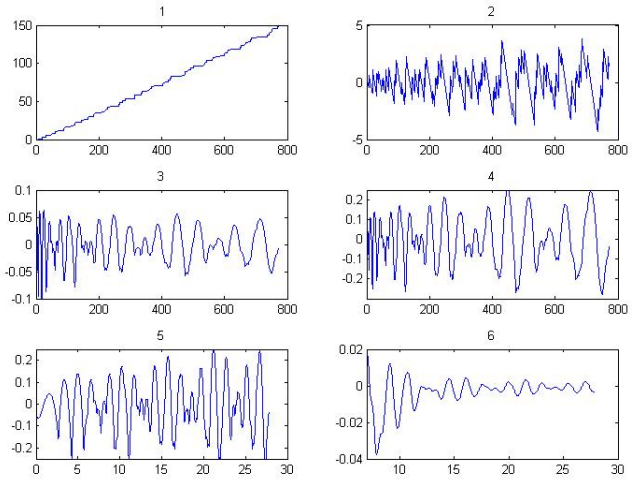

Figure 3.15

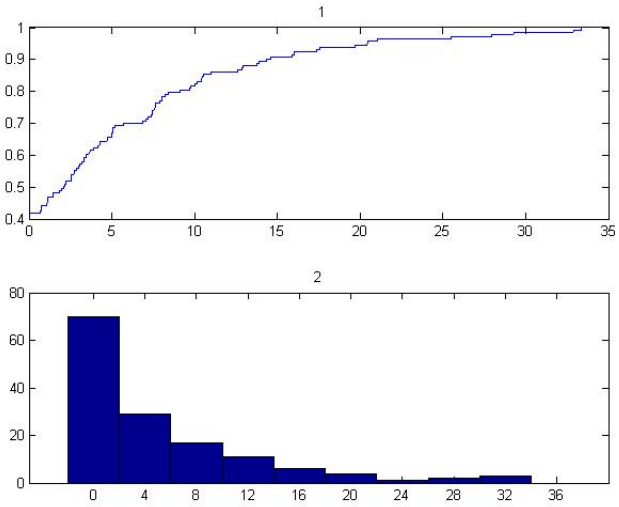

Figure 3.16

Example 3.8: Regular 6-pointed star with Dirichlet boundary conditions.

Here $\widetilde{N}(t) = \frac{s\sqrt{3}}{4\pi}t - \frac{3}{\pi}\sqrt{t} + \frac{25}{48}$. As in the case of the hexagon, Dirichlet eigenfunctions of the equilateral triangle extend by odd reflection, and there is a D_6 symmetry group. Therefore we again divide our table by $(\frac{4}{3}\pi)^2$ so that these eigenvalues become integers. The other eigenvalues of the hexagon do not, however, extend to the six-pointed star.

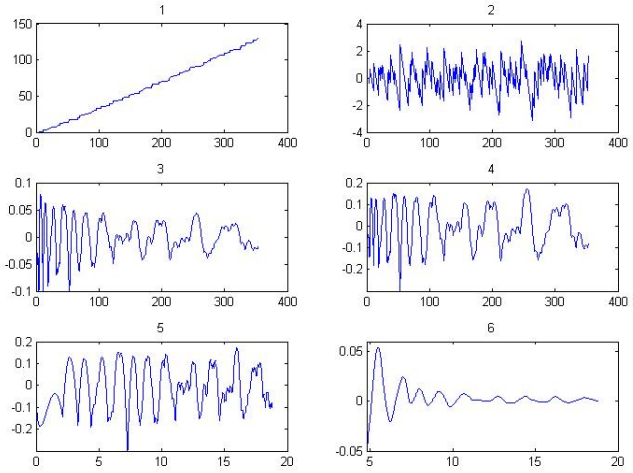

Figure 3.17

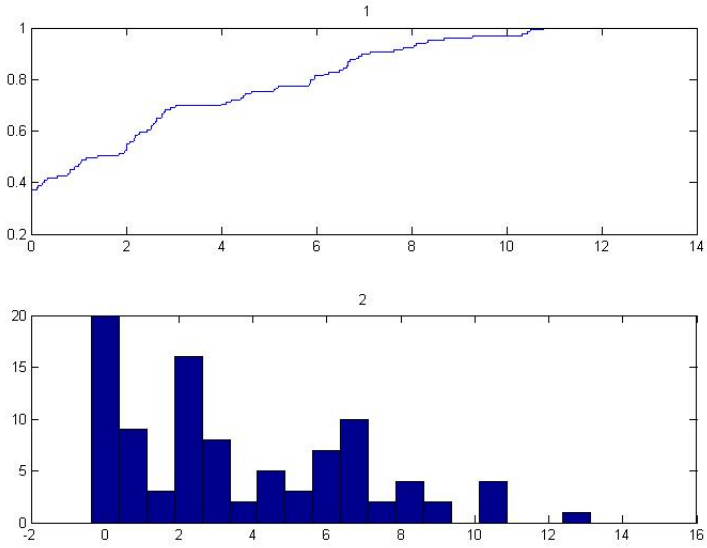

Figure 3.18

4 Hyperbolic Surfaces

In this section we discuss examples of surfaces in the hyperbolic plane of constant negative curvature -1. We use the upper half-plane model. In this model the Laplacian is given by

(4.1) $\Delta = \frac{1}{y^2}(\frac{\partial^2}{\partial x^2} + \frac{\partial^2}{\partial y^2})$

so the eigenvalue problem

(4.2) $-\Delta u = \lambda u$

is transformed into

(4.3) $-(\frac{\partial^2}{\partial x^2} + \frac{\partial^2}{\partial y^2})u(x,y) = \lambda y^2 u(x,y)$

and we used MATLAB to solve (4.3) on the surfaces with the appropriate boundary conditions. For simplicity we restricted our attention to Dirichlet boundary conditions, and our surfaces were either disks or triangles.

To describe triangles we recall theat geodesics in the upper half-plane model are either vertical half lines or half circles that intersect the x-axis perpendicularly. Without loss of generality we may take one side of the triangle to lie along the y-axis. Specifically, the triangle will have vertices $(0, y_1), (0, y_2)$ and (x_3, y_3), seen in figure 4.1 as points C, A, and B, respectively.

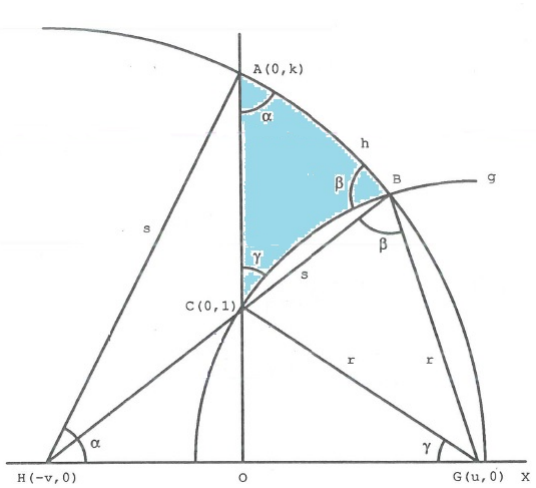

Figure 4.1

The two boundary circles are $y^2+(x-a_j)^2 = r_j^2$ for $j = 1, 2$, and (x_3, y_3) lies at the intersection of these circles, so $x_3 = \frac{r_2^2-r_1^2-a_2^2+a_1^2}{s(a_1-a_2)}$, $y_3 = \sqrt{r_1^2-(x_3-a_1)^2}$, and also $y_j = \sqrt{r_j^2-a_j^2}$ for $j = 1, 2$.

Since the model is conformal, the angles are the same as the Euclidean angles, so we have $\alpha_1 = \frac{\pi}{2} - \tan^{-1}(\frac{a_1}{y_1}), \alpha_2 = \frac{\pi}{2} - \tan^{-1}(\frac{-a_2}{y_2})$ and $\alpha_3 = \tan^{-1}(\frac{a_1-x_3}{y_3}) + \tan^{-1}(\frac{x_3-a_a}{y_3})$. The lengths of the opposite sides are $L_j = \frac{1}{2}log(\frac{r_j+a_j}{r_j-a_j}) - \frac{1}{2}log(\frac{r_j-x_x+a_j}{r_j+x_3+a_j}$ for $j = 1, 2$ and $L_3 = log\frac{y_2}{y_1}$. The area of the triangle is
$A = \iint_T \frac{dxdy}{y^2} = \frac{1}{r_2}(\cos^{-1}(\frac{-a_2}{r_2}) - \cos^{-1}(\frac{x_3-a_2}{r_2})) + \frac{1}{r_1}(\cos^{-1}(\frac{x_3-a_1}{r_1}) - \cos^{-1}(\frac{-a_1}{r_1})$.
Thus we have

(4.4) $\widetilde{N}(t) = \frac{1}{4\pi}At - \frac{1}{4\pi}(L_1+L_2+L_3)t^{\frac{1}{2}} + C$

for

(4.5) $C = -\frac{1}{12\pi}A + \frac{1}{24}\sum_{j=0}^{2}(\frac{\pi}{\alpha_j} - \frac{\alpha_j}{\pi})$

Of course everything may be expressed entirely in terms of the angles, since the angles determine the triangle. Thus the hyperbolic law of cosines yields

(4.6) $L_i = \cosh^{-1}(\frac{\cos\alpha_j\cos\alpha_k+\cos\alpha_i}{\sin\alpha_j\sin\alpha_k})$

for (i, j, k) any permutation of $(1, 2, 3)$, and the angle defect formula yields

(4.7) $A = \pi - (\alpha_1+\alpha_2+\alpha_3)$

Example 4.1: Hyperbolic Equilateral Triangles with Dirichlet boundary conditions.

We take $\alpha_1 = \alpha_2 = \alpha_3 = \frac{\pi}{k}$ for k an integer, $k \geq 4$. These triangles tesselate the hyperbolic plane. When k is even we may take odd reflections of the Dirichlet eigenfunctions to see that we are generating a subset of the collection of eigenfunctions on the hyperbolic closed manifolds $\Gamma\backslash SL(2,\mathbb{R})/SO(z)$ for the appropriate discrete subgroup Γ.

We show the results for $k = 4, 6$ in figures 4.2-3 and 4.4-5, respectively. Already for $k = 6$ the accuracy of our approximations begins to degrade. The website shows complete data for $k = 4, 5, 6, 7$.

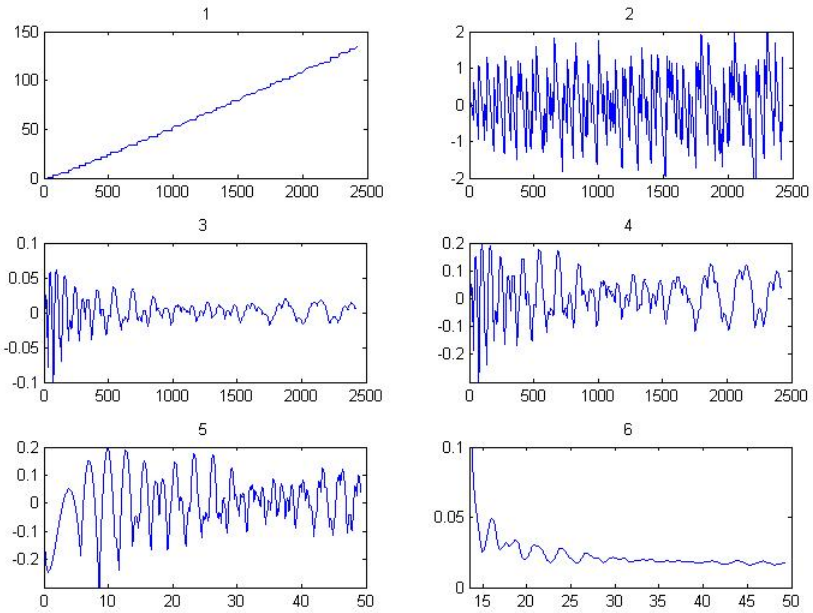

Figure 4.2

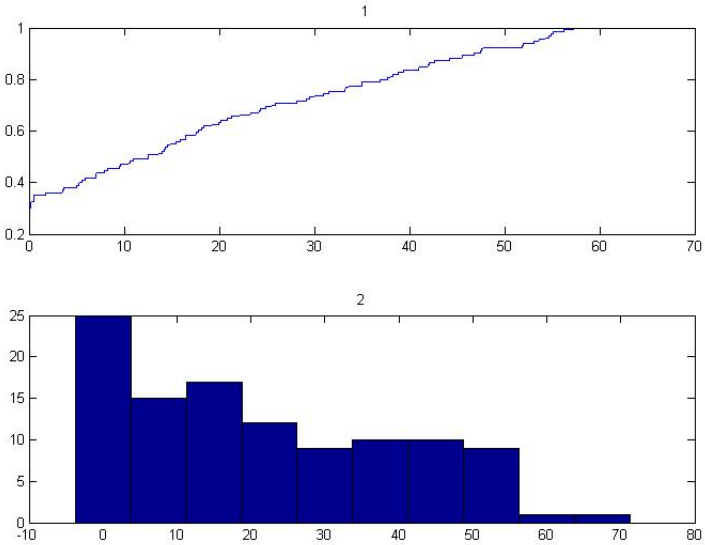

Figure 4.3

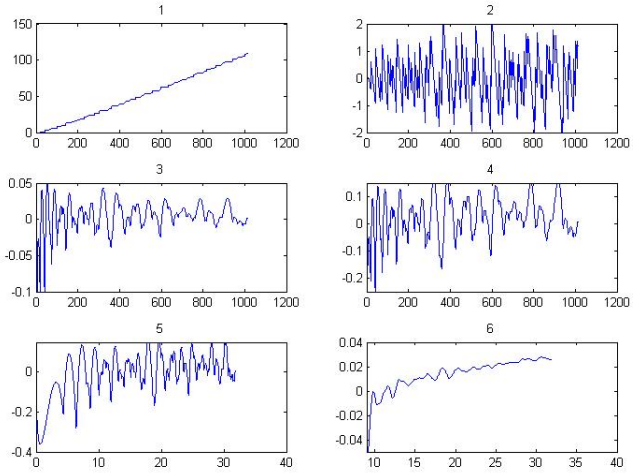

Figure 4.4

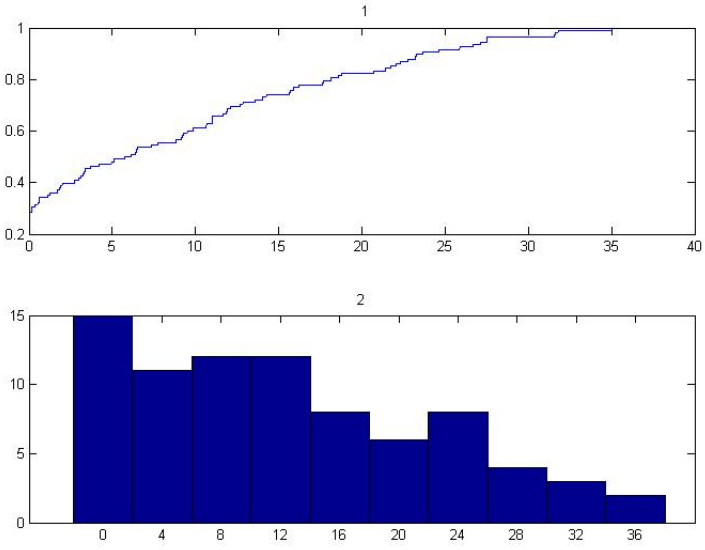

Figure 4.5

Example 4.2: General Hyperbolic Triangles with Dirichlet boundary conditions.

We present two hyperbolic triangles here with arbitrary measurements. Triangles are specified by a label (u, v, s) which correspond to the measuremnts in figure 4.1. Figures 4.6 and 4.7 correspond to $(5, 10, 11)$ and figures 4.8 and 4.9 correspond to $(3, 4, 6)$. Note that in the fifth and sixth counting graphs in figures 4.6 and 4.8 we begin to lose accuracy more quickly than we do in the Euclidean results. This is not unique to the arbitrary triangles, as it is present in both the hyperbolic equilateral triangles and hyperbolic discs, but it is especially noticeable here.

The complete results for more arbitrary hyperbolic triangles are shown on the website.

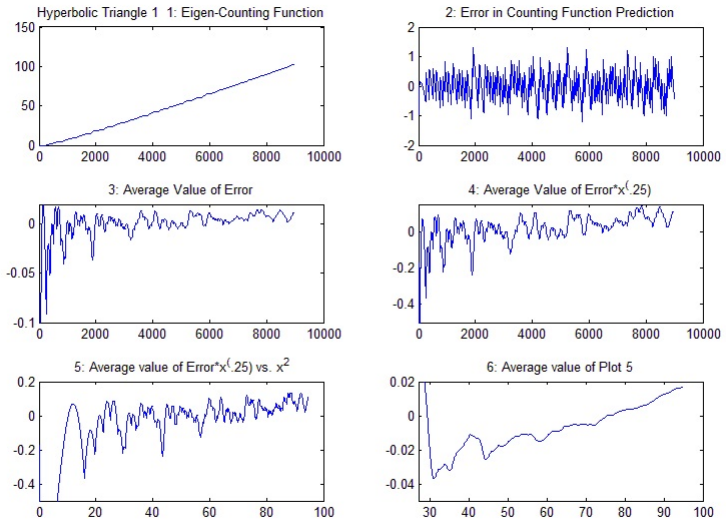

Figure 4.6

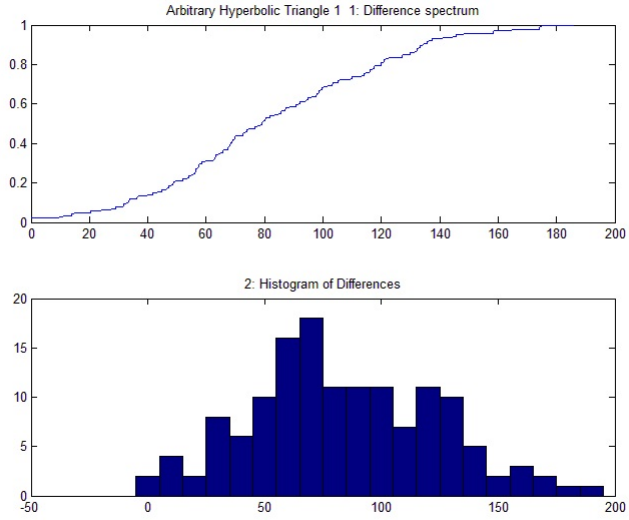

Figure 4.7

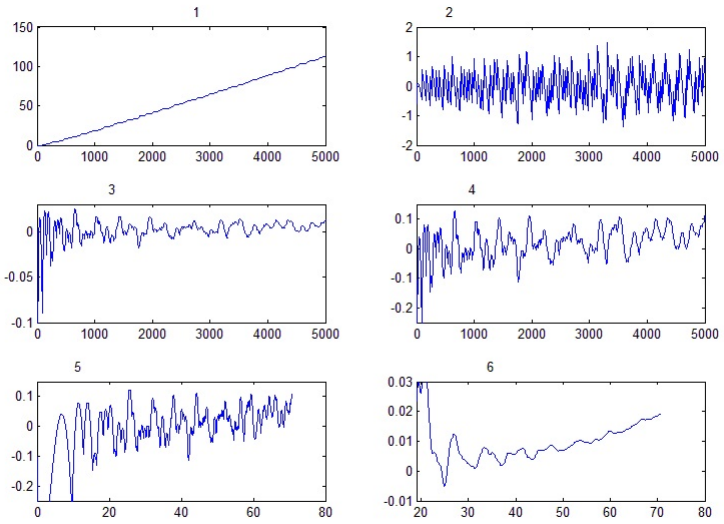

Figure 4.8

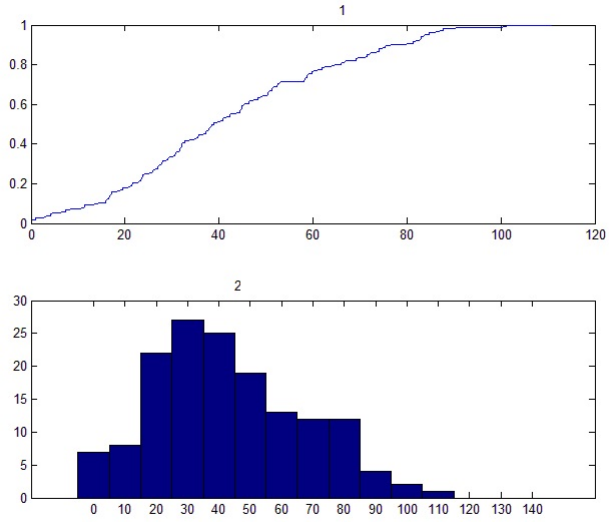

Figure 4.9

Example 4.3: Hyperbolic Discs with Dirichlet boundary conditions.

DESCRIPTION NEEDS TO BE WRITTEN: I'm presenting discs with r = 1, 1/2 in figures 4.10-11 and 4.12-13 respectively.

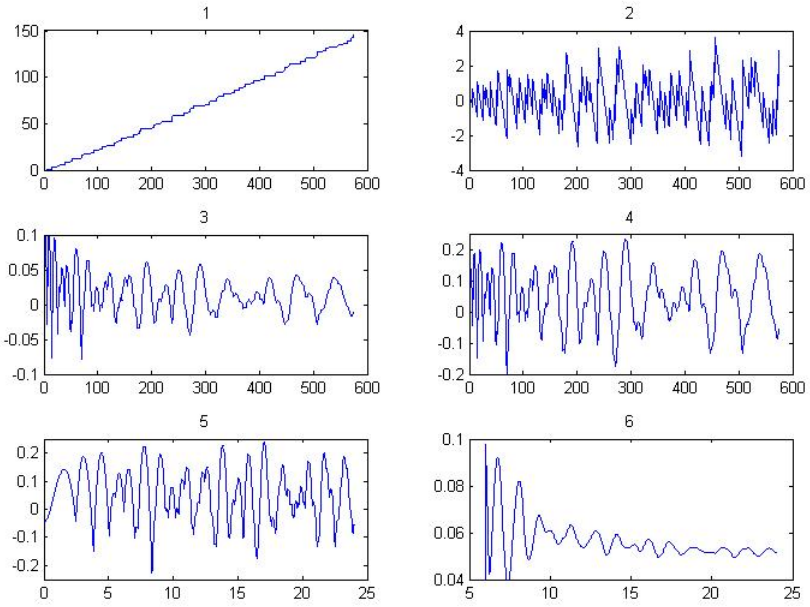

Figure 4.10

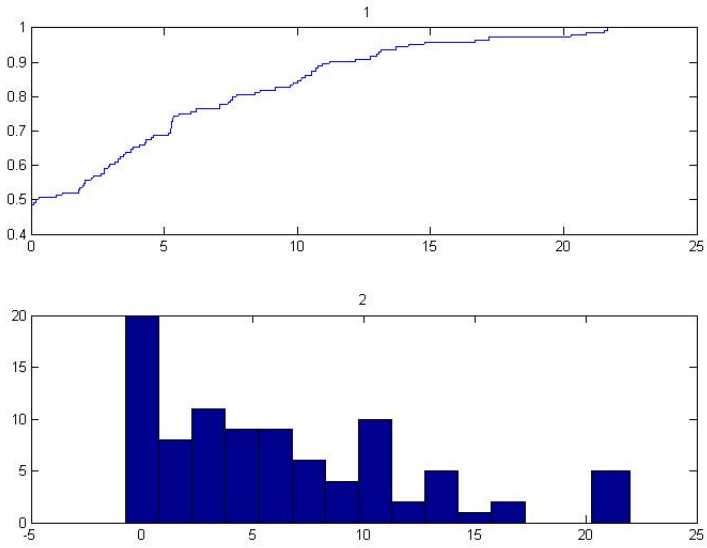

Figure 4.11

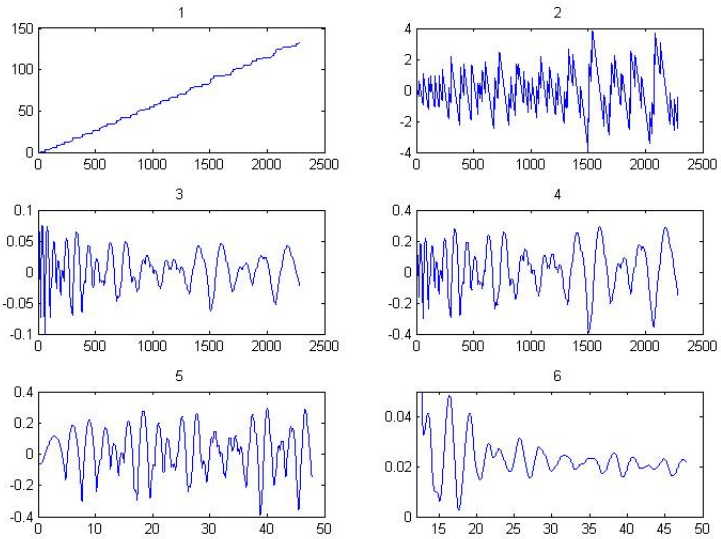

Figure 4.12

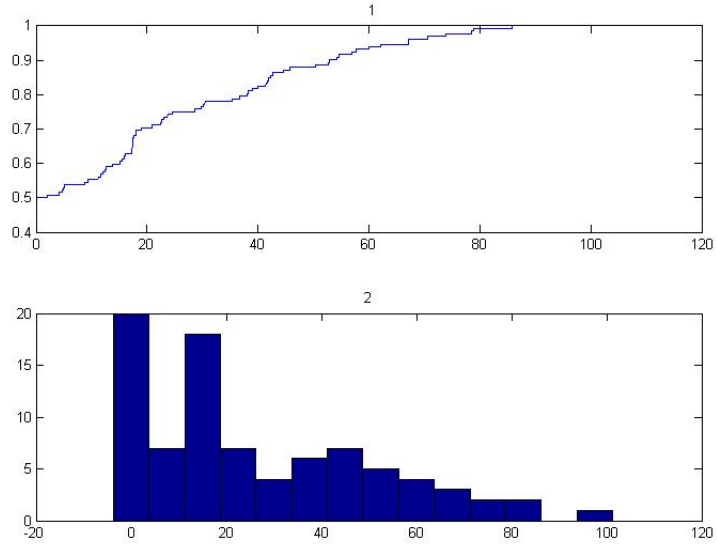

Figure 4.13

5 Spherical Surfaces

In this section we discuss examples of surfaces in the unit sphere (curvature $+1$). We use stereoprahic projection, placing the center of the sphere at $(0,0,1)$ and projecting from $(0,0,2)$ onto the (u,v) plane by $u = \frac{2x}{2-z}, v = \frac{2y}{2-z}$. The equator is mapped to the circle $u^2+v^2=4$, great circles through the poles are mapped to the lines through the origin, and other great circles are mapped to circles intersecting $u^2+v^2=4$ at two antipodal points. If we fix parameters to $t>0$ and β then these circles are given by $(u-t\sin\beta)^2+(v+t\cos\beta)^2 = t^2+4$ (intersecting $u^2+v^2=4$ at $\pm(2\cos\beta, 2\sin\beta)$).

We will consider triangles with vertices $(u_1,0),(u_2,0)$ and (u_3,v_3), with one edge along the u-axis and two edges being arcs of circles $(u-t_j\sin\beta_j)^2+(v+t_j\cos\beta_j)^2 = t_j^2+4$ for $j=1,2$. The angles of the triangle are given by
$\alpha_1 = \tan^{-1}(\frac{-u_1+t_1\sin\beta_1}{t_1\cos\beta_1})$
$\alpha_2 = \pi - \tan^{-1}(\frac{-u_2+t_2\sin\beta_2}{t_2\cos\beta_2})$
$\alpha_3 = \tan^{-1}(\frac{-u_3+t_2\sin\beta_2}{v_3+t_1\cos\beta_2}) - \tan^{-1}(\frac{-u_3+t_1\sin\beta_1}{v_3+t_1\cos\beta_1})$
The angles completely determine the triangle. The lengths of the sides are given by the spherical law of cosines

(5.1) $L_i = \cos^{-1}(\frac{\cos\alpha_i+\cos\alpha_j\cos\alpha_k}{\sin\alpha_j\sin\alpha_k})$

for (i,j,k) a permutation of $(1,2,3)$, and the area is given by the angle defect

(5.2) $A = (\alpha_1+\alpha_2+\alpha_3)-\pi$

The Laplacian is given by

(5.3) $\Delta = (\frac{u^2+v^2+4}{4})^2(\frac{\partial^2}{\partial u^2}+\frac{\partial^2}{\partial v^2})$

Example 5.1: Spherical Equilateral Right Triangle with Dirichlet boundary conditions.

This triangle serves as our main accuracy check for our calculated eigenvalues in spherical space. This is because it is a region for which the eigenvalue spectrum is known: the i^{th} distinct eigenvalue is equal to $4i^2+6i+2$ and has multiplicity i. We can see the first eigenvalues in Table 5.1 below, and Figures 5.1 and 5.2 are the same graphical analysis which we have previously used in the Euclidean and Hyperbolic cases.

	Initial	1	2	3	4	5	Predicted	True Value
1	12.16833	12.04264	12.01072	12.00269	12.00067	12.00017	12	12
2	30.92848	30.23554	30.05925	30.01484	30.00371	30.00093	30	30
3	31.10818	30.28025	30.07043	30.01764	30.00441	30.0011	30	30
4	58.89556	56.73392	56.18445	56.0462	56.01156	56.00289	56	56
5	59.60545	56.91078	56.22873	56.05728	56.01433	56.00358	56.00001	56
6	59.87166	56.97753	56.24543	56.06146	56.01537	56.00384	56.00001	56
7	97.16554	91.81109	90.45516	90.11402	90.02852	90.00713	90.00001	90
8	98.88888	92.23472	90.56026	90.14023	90.03507	90.00877	90.00001	90
9	99.74519	92.453	90.615	90.15393	90.0385	90.00963	90.00001	90
10	100.1208	92.55272	90.64036	90.16033	90.0401	90.01003	90.00002	90

Table 5.1

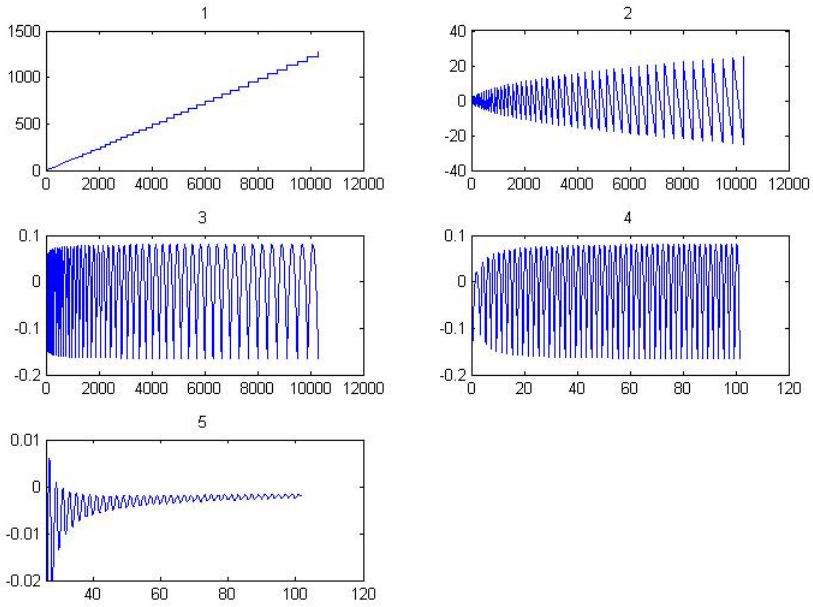

Figure 5.1

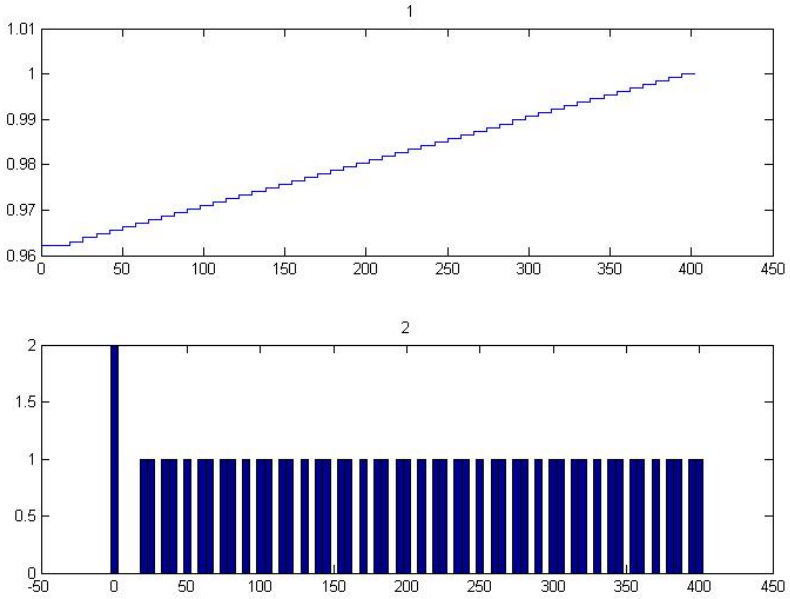

Figure 5.2

Example 5.2: General Spherical Triangle with Dirichlet boundary conditions.

We will now present a spherical triangle with arbitrary measurements. Spherical triangles are specified by a label $(t_1, \beta_1, t_2, \beta_2)$ which correspond to the measurements described above. Here we have $\widetilde{N}(t) = \frac{Area}{4\pi}t - \frac{\Sigma_{i=1}^{3} L_i}{4\pi}\sqrt{t} + (\frac{Area}{12\pi} + \frac{1}{24}\Sigma_{i=1}^{3}(\frac{\pi}{\alpha_i} - \frac{\alpha_i}{\pi}))$ The triangle corresponding to figures 5.3 and 5.4 is $(-1.5, \frac{\pi}{4}, -2, -\frac{\pi}{6})$. Note in the Figure 5.3 that while the accuracy of our calculated eigenvalues sufferes some decay, it does so at a slower rate than in the Hyperbolic surfaces.

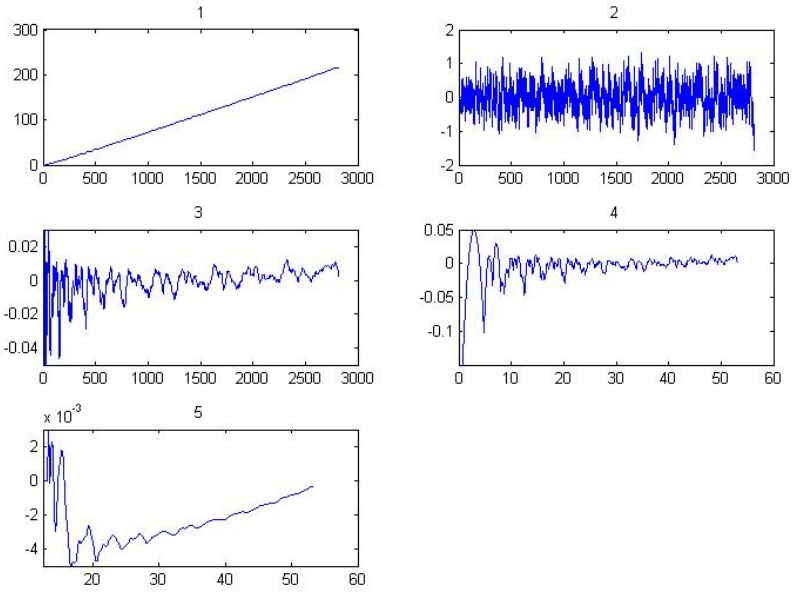

Figure 5.3

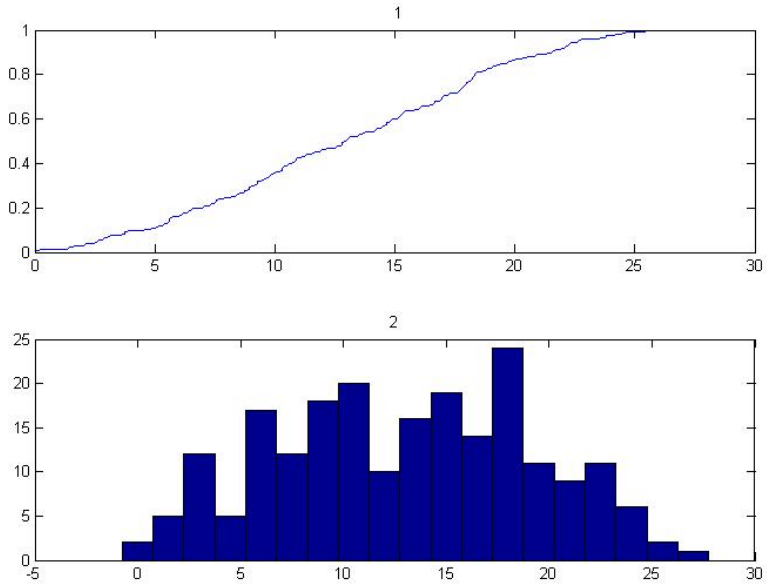

Figure 5.4

References

[B] P.M. Bleher, *Distribution of Energy Levels of a Quantum Free Particle on a Surface of Revolution*, Duke Math. J. Volume 74, Number 1 (1994), 45-93.

[S] R.S. Strichartz, *Average Error for Spectral Asymptotics on Surfaces*, preprint.

[M] T.S. Murray, *Spectral Asymptotics on Surfaces of Constant Curvature*, <http://www.math.cornell.edu/ tmurray3014/EigenIndex.html> (2015), Data Results Site